Enhanced Models of Heat Sources in Welding and Plasma Spraying (2-nd Report) - Examples of Thermal Plasma Models†

RONDA Jacek*, MURAKAWA Hidekazu**, NOGI Kiyoshi** and USHIO Masao**

Abstract

Several multi-scale models of thermal plasma produced both by arcs in TIG and PAW welding and used in plasma spraying are analyzed here from the perspective of mathematical modelling of the complex problem of energy transfer from the plasma to a work-piece. Such analysis is desirable before making a decision about the development of new software or a critical evaluation of available commercial software. The evaluation of transferred energy plays a key role in the numerical simulation of welding with solid phase transformations, analysis of hydrodynamic effects in a weld-pool, and simulation of micro-contacts of impinging granules and substrate in plasma spraying. Unfortunately, energy dissipation effects, which occur in a weld-pool, are omitted here and they require the further consideration. Simple one-dimensional theories are presented in the descriptive manner but multi-dimensional models of plasma are shown as schemes with tables of assumptions and boundary conditions.

KEY WORDS: (Thermal plasma) (Welding) (Plasma spraying) (Arc column) (Sheath) (Pre-sheath) (Momentum balance) (Energy balance) (Maxwell's equations) (Ohm's law) (Ampere's law) (Saha equation)

1 Introduction

The major objective of this report is to study the possibility for upgrading the heat source model used in welding and thermal spraying numerical simulation, the identification of necessary theoretical and analytical tools, and the evaluation of the effort and costs of the new codes related to the implementation of enhanced models of energy sources into existing commercial or our own codes. A better understanding of plasma modelling can be achieved by considering the multi-scale models and the corresponding identification of microscopic and macroscopic plasma parameters and state variables important for the plasma diagnostics and plasma generation techniques. Models of plasma sources applicable for welding are constructed for the simplified axisymmetric arc geometry and can be seen from the perspective of a sequential energy transfer from cathode (or anode) via an electric arc through weld-pool to HAZ. Considering this, the most complex model is proposed by Wendelstorf in [58] and Wendelstorf at. al. [57] where only two stages of energy transition: cathode-arc, and arc-anode are included and the process domain is split into five sub-regions: cathode sheath, cathode pre-sheath, arc column, anode pre-sheath, and anode sheath. Unfortunately, this model does not seem to be supported by any algorithm suitable for the solution of such complex plasma transition problem and only partial problem solutions are illustrating the author's modelling effort. The model proposed by Choo at. al. [9] consists of three stages of energy transition: cathode-arc, arc-anode surface, anode-weld pool. The domain is split into four regions: cathode surface, arc column, anode surface, and weld pool. The idea for the development of the algorithm is roughly the same as for the next model by Haidar at. al. The model proposed by Haidar at. al. [21] can be seen as the simplification of the previous one as it does not include the weld pool area but it offers very clear and simple strategy of the plasma problem solution, i.e. evaluation of eight plasma state variables: J_r, J_z, B_θ, V, v_r, v_z, P, h or T. The model for transferred plasma arc welding (PAW) proposed by Aithal at. al. consists only of two regions: flow within a torch, and external plasma jet. That model seems to be easy applicable for the development of our own software code. The simplest plasma model was proposed in the 1930's by Elenbaas [14] and Heller [25] for the axisymmetric case and suitable for the evaluation of the maximum plasma arc temperature.

The general rules and characteristics of thermal spraying are briefly presented here. Three mathematical models suitable for high-velocity oxygen-fuel (HVOF) and wire-arc spraying are considered. The simplest

†Received on November 18, 2002
*Professor, Wyzsza Szkola Techniczno-Ekonomiczna, Warszawa, ul. Hafciarska 11, Poland
**Professor, JWRI, Osaka

Transactions of JWRI is published by Joining and Welding Research Institute of Osaka University, Ibaraki, Osaka 567-0047, Japan

one-dimensional model proposed by Joshi at. al. [31] is suitable for HVOF spraying. The wire-arc spray model proposed by Kelkar at. al. [32] includes the arc model and plasma jet model with the consideration of particle breakup and transport model. The most complex model of plasma-injected particle interaction is proposed by Proulx at. al. [47].
This paper is the continuation of the review of magneto-hydro-dynamic (MHD) plasma theories given in [49].

2 Plasma Characteristics and Generation

2.1 Plasma characteristics

2.1.1 Plasma parameters

Plasma can be characterized by microscopic and macroscopic parameters

Parameter	Refers to
microscopic	interactions between individual particles
macroscopic	specific plasma properties in a continuum that can be described by the basic MHD equations

The most important macroscopic plasma parameters are

Parameter	Definition
Langmuir plasma frequency (harmonic oscillations)	$\omega_{pe} = (4\pi n^{(e)} e^2/m^{(e)})$ $= 5.64 \times 10^4 n^{(1/2)}$; $[rad/s]$
Debye screening length of the potential V	$\lambda_D = (kT/4\pi n^{(e)} e^2)^{1/2}$ $= 7.43 \times 10^2 T^{1/2} n^{-1/2}$; $[cm]$
Landau length (critical length)	$l_L = e^2/kT$
Collision path length (mean free path length)	$\lambda = \frac{0.6\times 10^6 T^2}{n^{(e)} \ln(\lambda_D/l_L)}$ $\approx \frac{1.3\times 10^4 T^2}{n^{(e)}}$
Collision frequency (collision probability) or in terms of the collision cross-section	$\nu_c = \tau^{-1} = \frac{\bar{v}}{\lambda}$ $\nu_c = n^{(e)} \bar{v} \sigma(v)$

Where the meaning of each parameter is given below

- Langmuir frequency
  - The natural collective oscillation frequency of a charged species: electrons, or ions, in a plasma, in the absence of a magnetic field or at least parallel to that field.
- Debye screening length,
  - The characteristic distance over which charges are shielded in a plasma. Debye length is also the ratio of thermal velocity to plasma frequency.
- Landau length
  - The Landau length specifies the mean distance l_{pp} between plasma particles to prevent recombination of ions and electrons, i.e. $l_{pp} > l_L$. The condition, $l_{pp} > \lambda_D$, means that there is no plasma, because of the lack of cooperative interaction between particles. A plasma exists when $l_L < l_{pp} < \lambda_D$.
- Collision path length,
  - Average distance that a particle travels between collisions. The mean free path is $\approx \frac{1}{\sigma(v) n^{(e)}}$.
- Collision frequency
  - Collision frequency, ν_c, for the Maxwellian distribution of velocity is such that $\frac{\nu_c}{\omega_{pe}} \approx \frac{\lambda_D}{\lambda}$, under equilibrium conditions.

2.1.2 Plasma diagnostics

For decades the confrontation between theory and experiments has driven the development of plasma science. The correct experimental identification of plasma states and parameters is the milestone in the development of plasma theory. The basic understanding of plasma diagnostics can be provided by e.g. [30]. Plasma state variables: temperature, enthalpy, velocity, and density, can be measured by complex instruments. Only the general ideas of measurement techniques for state variables are mentioned here. Techniques for plasma diagnostics are described in a number of papers, eg. [55], [56]. The measurement methods can be split in two groups: plasma diagnostics, and particle diagnostics. In plasma diagnostics

- plasma temperature can be
  - measured assuming LTE and using atomic or molecular spectroscopy, applicable only when $T > 6000K$,
  - and deduced from the integrated volumetric emission coefficient $\varepsilon_L(\lambda_0)$ of suitable emission lines for "plasma gas" (eg. nitrogen or argon). The local emissivity is obtained from the observed side-on intensity I_L by Abel's inversion [24].
- plasma velocity can be determined by several techniques:
  - enthalpy probe and Pitot tube [7], [12], [19],
  - laser Doppler anemometry - optical method [13], [17], [37], [38],
  - measurement of particle velocities "in situ" (i.e. in correct place) by using a spatial filter for particles radiating light [35],
  - cross-correlation method based on the measurement of travel time [24],

Techniques for determination of particle velocity, particle temperature, and number densities are

- velocity measurements
  - Mach probes [30],
  - laser-induced fluorescence [46]
- enthalpy and velocity
  - Pitot probe technique [7],
- particle temperature
  - two color pyrometry at two wavelengths [55] for plasma with seeding particles,
  - spectroscopic method [20],
  - electron temperature along the plasma column determined using a modified Saha equation and a corrected Boltzmann-plot after providing argon upper excited states remaining in excitation saturation balance [36],
- number densities
  - Rayleigh scattering of argon-ion laser radiation [15]
- electron temperature and electron density
  - Thomson laser scattering [18],

2.2 Plasma generation

There are three basic kinds of plasma dischargers: arc, glow, and corona. Typical physical conditions for generation of such plasmas are listed below

Conditions	Arc	Glow	Corona
Frequency [MHz]	$0-40$	$0-40$	$0-40$
Power [KW]	$(1-20)10^3$	$0.1-100$	$0.1-200$
Flow rate [kg/s]	0	10^{-6}	10^{-6}
Electron concentration $[m^{-3}]$	10^{20}	$10^{15}-10^{18}$	10^{12}
Electric field strength [V/m] (intensity of) (electric field)	2×10^3	$5\times10^3-10^5$	2×10^6
Pressure $[N/m^2]$	$\frac{4}{3}\times10^4$	$\frac{4}{3}\times10^4$	$\frac{4}{3}\times10^4$
Electron temperature [K]	10^4	10^4	10^4
Atom temperature [K]	10^4	7×10^2	7×10^2
Degree of homogeneity	moderate	high	low

There are two basic mechanisms to initiate ionization:

Forms of energy transfer	Mechanisms of ionization
application of heat with substantial temperature increase	collisional ionization, photo ionization due to electromagnetic radiation in the hot gas,
radiation or electric current without substantial temp. increase,	particle radiation electromagnetic radiation formation of electrical current in gas

Couplings of these two mechanisms frequently occur in technical generation of plasma. Methods of plasma generation based on such mechanisms can be classified in four categories:

Method of plasma generation	Description
through application of heat [50]	King's plasma furnace, Q-engine,
through compression	ballistic compressor
by radiation	electron beam focused on on a diluted gas produces plasma
by electric current (gas dischargers)	by formation of electric current in gas: glow dischargers, arc dischargers,

Arc discharge generators, following [53], can be divided into three categories:

Generators	Type of arc	Attributes	Application
electrode plasma (EP)	non-transferred	low voltage	spraying welding melting low velocity gas heating
		high voltage	operations with high pressure hydrogen heating spraying
electrode plasma (EP)	transferred	direct work heating	welding cutting melting surfacing
electrode plasma (EP)	secondary electrode		spraying gas heating
electrode-less plasma (ICP)		low frequency	high power gas heating particle heating
		high frequency	low power gas heating particle heating spraying high resistivity gases high pressure
hybrid	ICP super-imposed on EP		particle heating gas heating

3 Plasma Arc Models in Welding

A simple arc model [14] and [25] invented in the 1930s together with three complex thermal plasma theories for TIG welding shown in [9], [51] and [57] and one for plasma arc welding (PAW) described in [2] can be identified in the literature as the most welding-engineering oriented models. More complex theories are presented here in the form of schemes with equations and relations expressing the continuity of fluxes and balances of energy transmission from the cathode (or anode - PAW) to HAZ. Fundamental assumptions and appropriate boundary conditions are listed in tables for each presented theory.

3.1 Simple model of arc column

A simple model for the arc column [14] and [25] was based on equating a temperature gradient term $div(-\kappa^{(e)}\nabla T)$ with one related to the generation of an electric field σE^2. Thermal diffusion and effects of radiation were neglected in that model. The basic equation for the axisymmetric case took the form

$$\frac{1}{r}\frac{d}{dr}(r\kappa^{(e)}\frac{dT}{dr}) + \sigma E_z^2 = 0 \qquad (1)$$

Introducing the heat flux potential $S = \int_0^T \kappa^{(e)} dT$, Eq.(1) can be express as

$$\frac{1}{r}\frac{d}{dr}(r\frac{dS}{dr}) + \sigma E_z^2 = 0 \qquad (2)$$

where $S(T)$ is the function of temperature only. Integrating Eq.(2) and using Ohm's law $I = 2\pi E_z \int_0^R \sigma r dr$, the solution obtained by the method of characteristics, following [39], can be shown in the form:

$$E = \frac{1.08}{R}(\frac{2fS_0}{\sigma_0})^{\frac{1}{2}} e^{\frac{1}{2zf}} \qquad (3)$$

$$I = 7.27R(2fS_0\sigma_0)^{\frac{1}{2}} e^{-\frac{1}{2zf}}, \qquad (4)$$

where $f = \frac{\int_0^{S_0}\sigma dS}{\sigma_0 S_0}$. Following the above solution and [24], it can be deduced that

$$EI = f_1(S) = f_2(T) \qquad (5)$$

and therefore the maximum temperature $T_{max} = f_2^{-1}(EI)$ is a function of the power input per unit length $L = IE$. This means that the maximum temperature of a plasmatron appears to be limited only by the power input as opposed to a flame torch where the maximum temperature is limited by the internal enthalpy of the combustion gas.

3.2 Scheme of TIG and plasma arc model proposed by Wendelstorf, Decker, Wohlfahrt and Simon [57]

Physical regions of the thermal plasma model proposed by Wendelstorf, et. al. [57] are shown in **Fig. 1**.

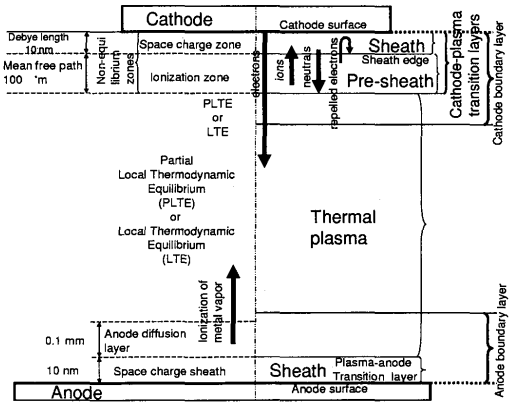

Fig.1 Physical regions in TIG arc

The fundamental assumptions for this model are extracted in the following table

	Arc column
1	the fluid flow is laminar and $Re < 400$
2	the fluid flow at arc fringes can become turbulent (in MHD theory sense)
3	is in local thermodynamic equilibrium (LTE)
4	is quasi neutral, i.e. free of space charges
5	the fluid flow is 2-D in cylindrical coordinates (r, z)
	Cathode region
1	electron temperature $T^{(e)}$ is equal to the heavy particle temperature $T^{(i)}$
	Pre-sheath
1	this zone is quasi-neutral
2	two-fluid flow is appropriate
3	radiation losses can be neglected
4	thermal pressure is constant and equal to the atmospheric
	Sheath
1	ions are mono-energetic
2	is collision free
3	field emission is negligible
4	ions re-combine at the cathode surface
5	velocity distribution of electrons at the sheath-edge is Maxwellian
	Anode region
1	appreciable deviations from LTE prevails throughout the zone
2	modelling of anode layer is similar to the cathode modelling
3	excess pressure (deduced from the column modelling) is constant within the zone

The flow problem for plasma species and the energy transmission consists of equations depicted in **Fig. 2** and **Fig. 3.**

The boundary conditions are given originally only for the transition from the cathode to LTE (or PLTE) thermal plasma and can be listed as follows

Arc subregion	T	P
arc plasma - far from cathode surface	$T_P = 21000K$ $\frac{dT_P}{dx} = -2.7 \cdot 10^7 k/m$	
Pre-sheath		$1.013 \cdot 10^5 Pa$
cathode surface	either $T_c = 3000K$	

The additional conditions for this model are

Arc subregion	d_{dot}	Φ_c	J_{tot}
pre-sheath	$1 \cdot 10^{-4}$ m		
cathode surface		2.63eV	$1.2 \cdot 10^8 A/m^2$

3.3 Scheme of TIG and plasma arc approved-model proposed by Haidar and Lowke [21] and Sansonnens, Haidar and Lowke [51]

The plasma arc model proposed by Haidar and Lowke [21] and Sansonnens, Haidar and Lowke [51] is illustrated by the scheme in **Fig. 4** where balance equations and continuity requirements are appropriate for the single-fluid MHD model. Boundary conditions for the arc column, depicted in **Fig. 5**, are listed below

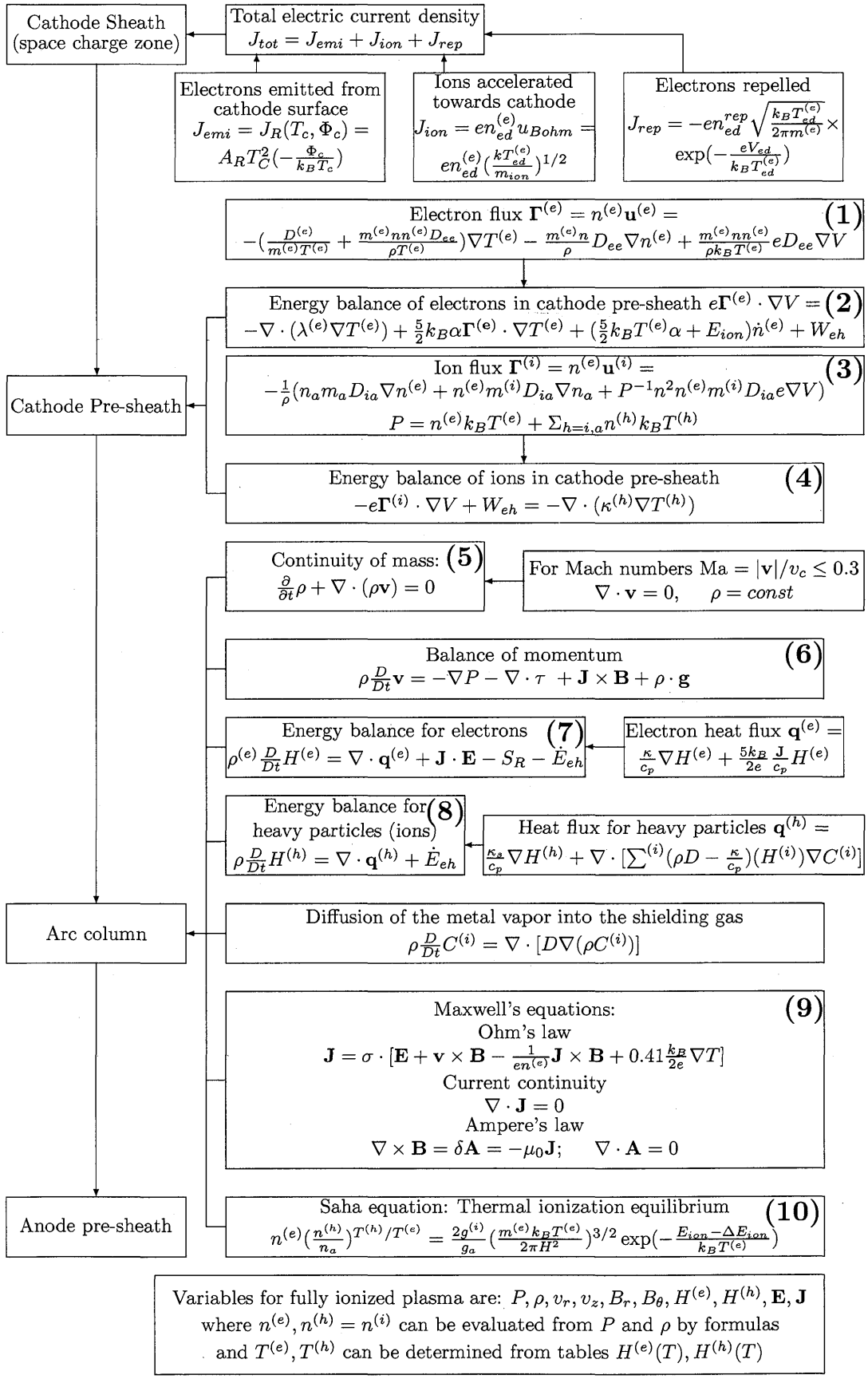

Fig. 2 The first part of the scheme of TIG plasma arc model proposed by Wendelstorf, Decker, Wohlfahrt, and Simon [57] and [58]

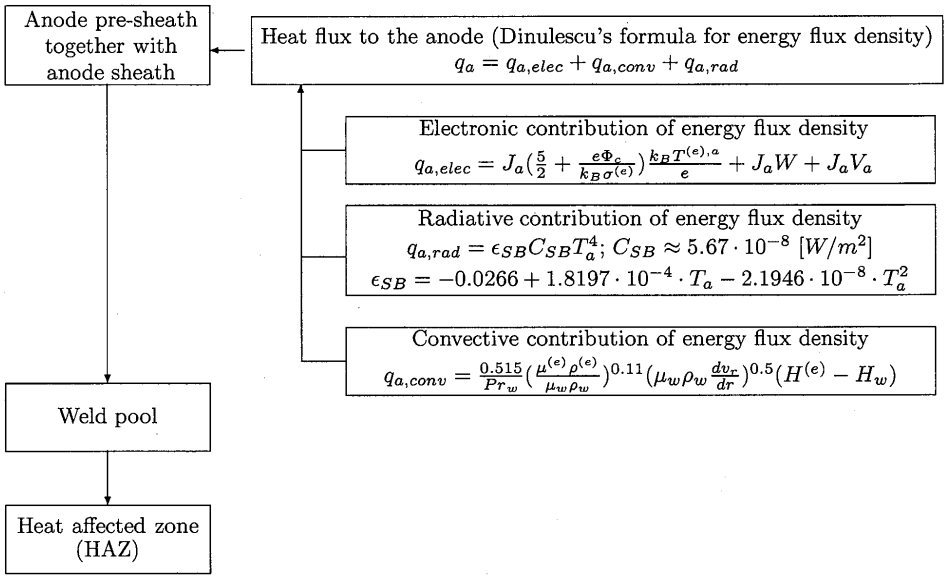

Fig. 3 The second part of the scheme of TIG plasma arc model proposed by Wendelstorf, Decker, Wohlfahrt, and Simon [57] and [58]

Subregion	v_r	v_z	T	V	P
A^aB^a	0	$\frac{\partial v_z}{\partial r}$	$\frac{\partial T}{\partial r} = 0$	$\frac{\partial V}{\partial r} = 0$	
B^aC^a					0
C^aD^a		v_{gif}			
E^aF^a			300 K		
F^aG^a			300 K		
G^aH^a			300 K		
H^a					101 kPa
within BCDEOB^a					

Subregion	J_z	$n^{(e)}$
A^aB^a		$\frac{\partial n^{(e)}}{\partial r} = 0$
B^aC^a	$n^{(e)} = \frac{J_R}{ev_{th}}$	$\lvert J_R\rvert = AT^2 \exp(-\frac{\Phi^{(e)}e}{k_B T})$
C^aD^a		$v_{th} = (\frac{8k_B^T}{\pi m^{(e)}})^{1/2}$
D^aE^a	$\star$	
within BCDEOB^a		0
$\star$ indicates the assumption of uniformity of J_z over the circular plane at the cold top face of the cylindrical cathode		
in addition it is assumed that within BCDEOB $D^{(e)} = 0$		

The boundary conditions for the weld-pool are

Weld pool subregion	v_r	v_z	T	V	p	J_z	$n^{(e)}$
C^pD^p				0			
within ABCDEFA^p							0
in addition within BCDEOB $D^{(e)} = 0$							

Equations used in **Fig.4** are denoted by the following symbols:

Acronym in the scheme for Haidar and Lowke model [21]	Equation
ECC	electron current continuity
CD	current density
CC	current continuity
TCD	total current density
MC	mass continuity
AMC	axial momentum conservation
RMC	radial momentum conservation
EC	energy conservation

The rough idea of the strategy for the solution of the plasma problem formulated by Haidar and Lowke [21], and by Sansonnens, Haidar and Lowke [51] is described in [34] and can be listed as follows:

- Substitute
$$J_r = -\sigma\frac{\partial V}{\partial r} + eD^{(e)}\frac{\partial n^{(e)}}{\partial r} \tag{6}$$
to
$$\frac{1}{r}\frac{\partial}{\partial r}(rJ_r) + \frac{\partial}{\partial z}(J_z) = 0, \tag{7}$$
- Substitute
$$J_z = -\sigma\frac{\partial V}{\partial z} + eD^{(e)}\frac{\partial n^{(e)}}{\partial z} \tag{8}$$
to Eq.(7),
- Then V becomes the only unknown in the following Eq.
$$-\sigma(\frac{1}{r}\frac{\partial V}{\partial r} + \frac{\partial^2 V}{\partial r^2} + \frac{\partial^2 V}{\partial z^2}) + eD^{(e)}(\frac{1}{r}\frac{\partial n^{(e)}}{\partial r} + \frac{\partial^2 n^{(e)}}{\partial r^2} + \frac{\partial^2 n_e}{\partial z^2}) = 0, \tag{9}$$
- solve Eq.(9) for V,
- changing potential V evaluate J_r from (6) and J_z from Eq.(8),
- knowing J_r and J_z evaluate B_θ from
$$\frac{1}{r}\frac{\partial}{\partial r}(rB_\theta) = \mu_0 J_z, \tag{10}$$

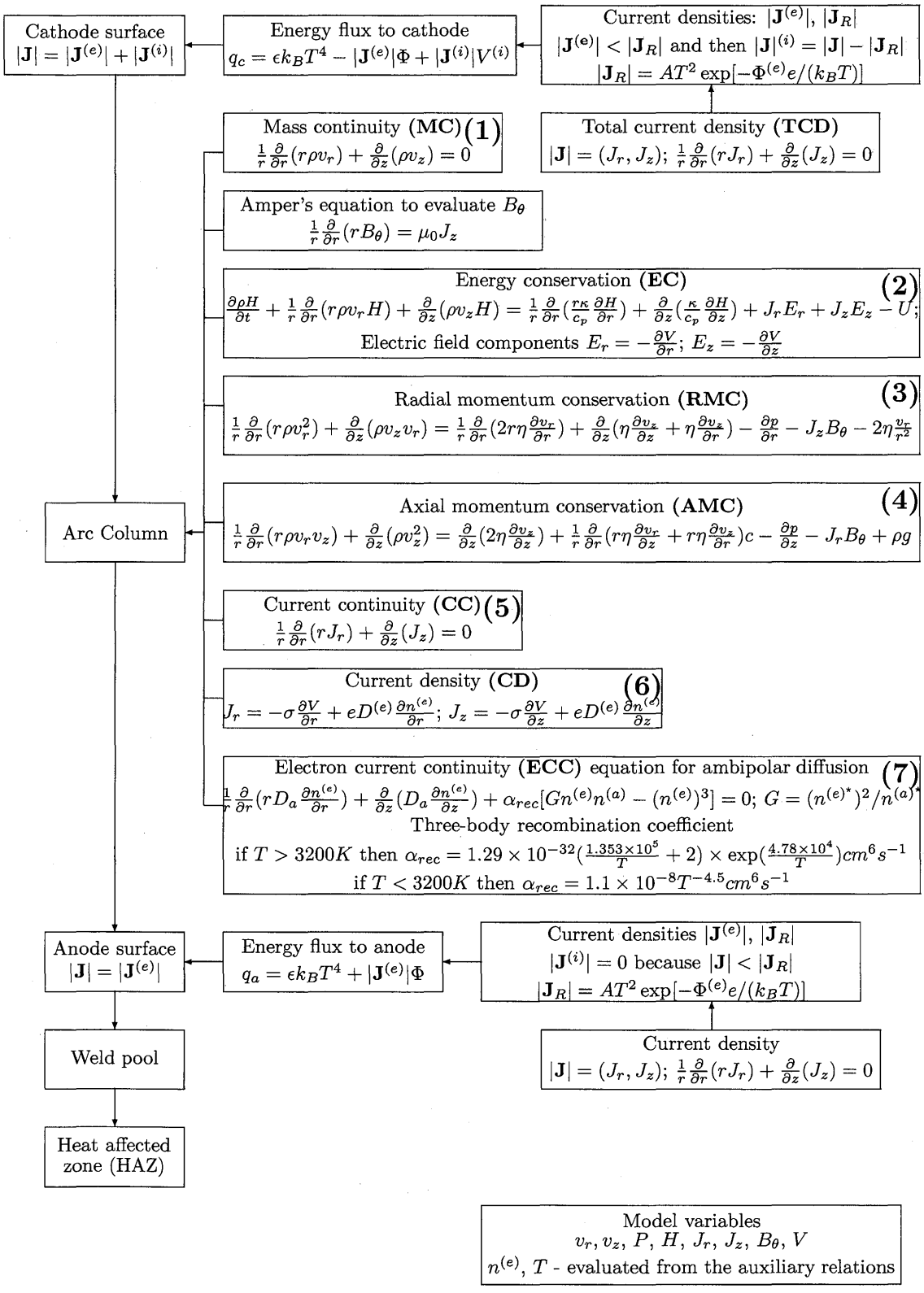

Fig. 4 Scheme for the model of thermal plasma for TIG welding proposed by Haidar and Lowke [21] and Sansonnens, Haidar and Lowke [51]

- knowing J_r, J_z and B_θ evaluate velocities v_r, v_z and pressure P from

  - mass continuity equation

$$\frac{1}{r}\frac{\partial}{\partial r}(r\rho v_r) + \frac{\partial}{\partial r}(\rho v_z) = 0 \qquad (11)$$

  - radial momentum conservation equation

$$\frac{1}{r}\frac{\partial}{\partial r}(r\rho v_r^2) + \frac{\partial}{\partial z}(\rho v_z v_r) = -\frac{\partial P}{\partial r} - J_z B_\theta + \frac{1}{r}\frac{\partial}{\partial r}(2r\eta\frac{\partial v_r}{\partial r}) + \frac{\partial}{\partial z}(\eta\frac{\partial v_r}{\partial z}) + \eta\frac{\partial v_z}{\partial r} - 2\eta\frac{v_r}{r^2}, \qquad (12)$$

  - axial momentum conservation equation

$$\frac{1}{r}\frac{\partial}{\partial r}(r\rho v_z v_r) + \frac{\partial}{\partial z}(\rho v_z^2) = -\frac{\partial P}{\partial r} - J_r B_\theta + \frac{\partial}{\partial z}(2\eta\frac{\partial v_z}{\partial z}) + \frac{1}{r}\frac{\partial}{\partial r}(r\eta\frac{\partial v_r}{\partial z}) + r\eta\frac{\partial v_z}{\partial z} + 2\rho g, \qquad (13)$$

- knowing v_r, v_z, J_r, J_z evaluate enthalpy h from the energy conservation equation

$$\frac{1}{r}\frac{\partial}{\partial r}(r\rho v_r h) + \frac{\partial}{\partial z}(\rho v_z h) = \frac{1}{r}\frac{\partial}{\partial r}(\frac{r\kappa}{c_p}\frac{\partial h}{\partial r}) + \frac{\partial}{\partial z}(\frac{\kappa}{c_p}\frac{\partial h}{\partial z}) + J_r E_r + J_z E_z - U, \qquad (14)$$

- knowing enthalpy h define temperature T,
- knowing T calculate the new values of plasma transportation parameters gtd(T),
- substitute the new plasma transportation parameters to Eq.(9),
- solve Eq.(9) for V,
- repeat next steps with Eqs.(11), (12), (13), (14) until the solution of Eq.(9),
- repeat all steps until $t \leq t_f$.

Data and unknowns for the problem formulated by Haidar and Lowke [21], and by Sansonnens, Haidar and Lowke [51] are the following

Data	
initial enthalpy	h_0
electron number density defined from the graph for argon obtained for the quasi-static solution assuming LTE for plasma	$n^{(e)}$
Unknowns	
pressure	P
velocity	v_r, v_z
current density	J_r, J_z
magnetic field	B_θ

The effective algorithm for the solution of the plasma problem stated in [21] and [51] was proposed by [43], [44] [45] and [54]. The solution technique is known as the volume-control method, and is one of the first examples of using the finite-volume method in fluid dynamics.

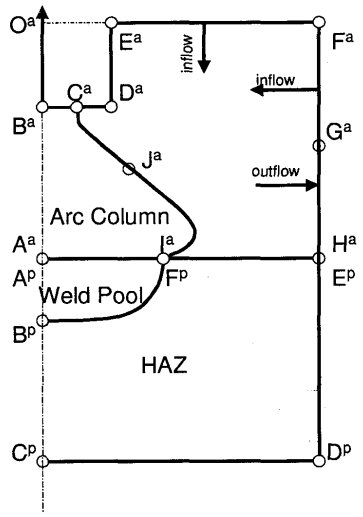

Fig. 5 Boundary conditions for the model proposed by Haidar and Lowke [21] and Sansonnens et. al. [51]

3.4 Scheme of TIG arc model proposed by Choo, Szekely and Westhoff [9]

The welding problem formulated and solved by Choo, Szekely and Westhoff in [9] is the most complex and covers the problem of energy transfer from the arc column to both the weld pool and the cathode surface. The fundamental assumptions for the weld pool model are given in the following table

1	the weld pool is small and thus the laminar flow assumption is appropriate
2	the surface is a gray body
3	the surface tension is a linear function of temperature
4	physical, electrical and transport properties of liquid and solid parts of a weld pool are constant and independent of temperature
5	upper boundary on liquid temperature is 500 K below the boiling point

and the assumptions for modelling of the TIG arc are listed below

1	the arc is radially symmetric
2	the arc is in steady-state conditions
3	the arc is in local thermodynamic equilibrium i.e. temperatures of heavy particles and electrons are not significantly different
4	the arc plasma consists of pure argon at atmospheric pressure
5	the effect of metal vapor from electrode and workpiece is neglected
6	the flow is laminar
7	the plasma is optically thin so that radiation may be accounted for using an optically thin radiation loss per unit volume
8	the heating effect of viscous dissipation is neglected
9	buoyancy forces due to gravity are neglected

The governing equations for the theory of welding arc with a deformed anode surface are listed in schemes

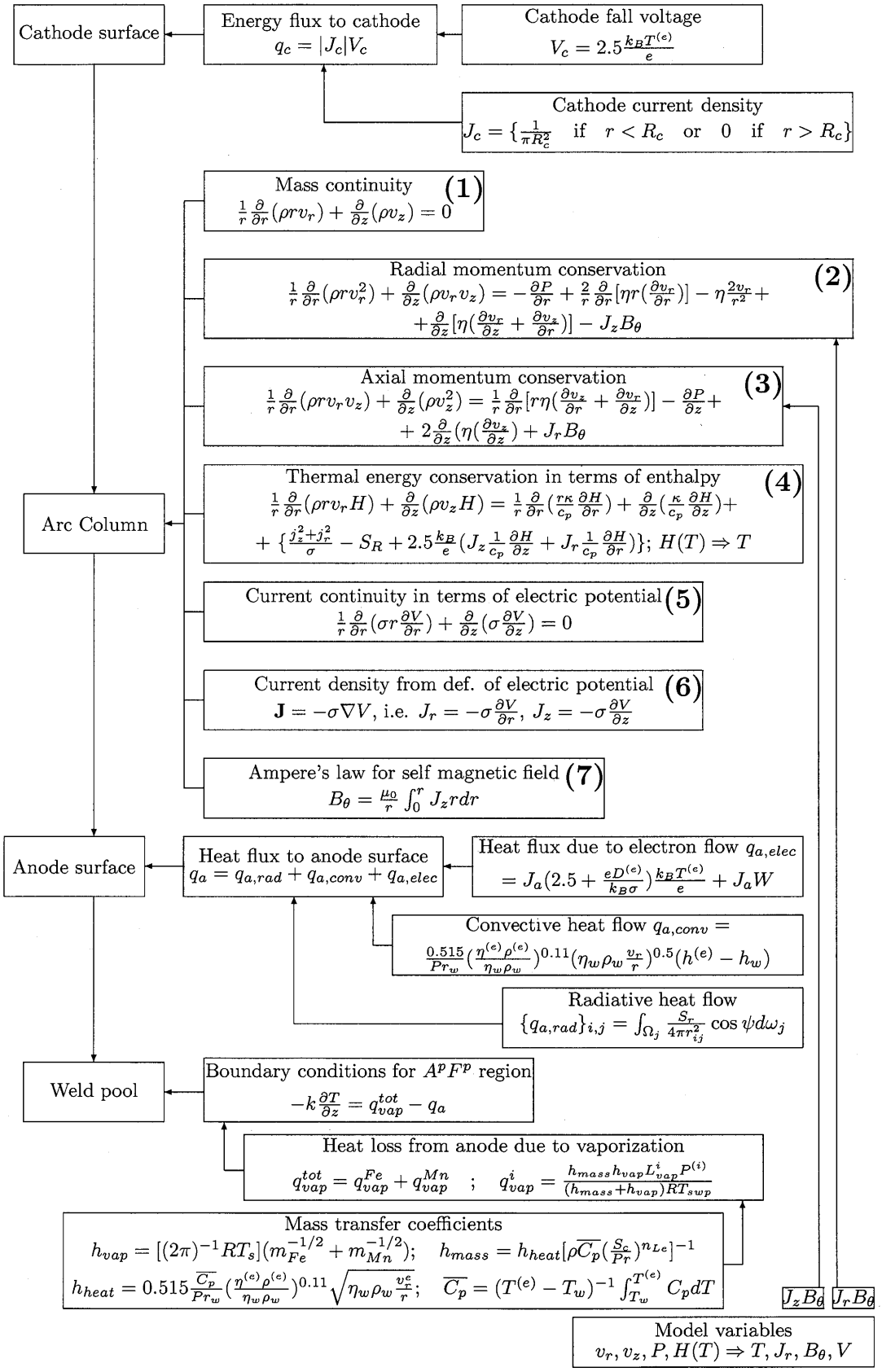

Fig. 6 The first part of the scheme for the model of thermal plasma for TIG welding proposed by Choo, Szekely and Westhoff [9]

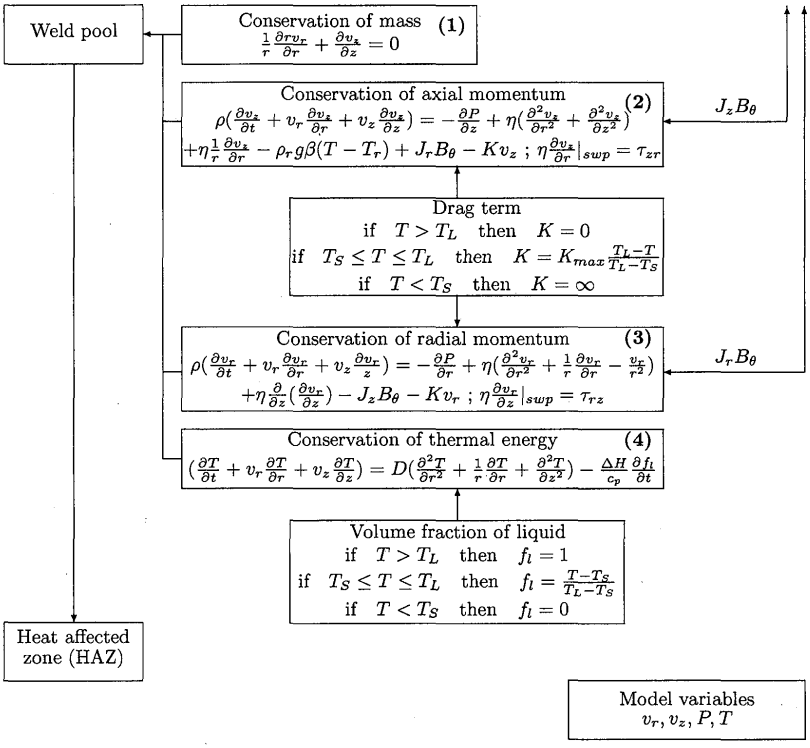

Fig. 7 The second part of the scheme for the model of thermal plasma for TIG welding proposed by Choo, Szekely and Westhoff [9]

shown in **Fig. 6** and **Fig. 7**.

The boundary conditions for the arc model subregion in terms of $(\mathbf{v}^{(a)}, h^{(a)})$ or $(T^{(a)}, V)$ and the weld pool model subregion $(\mathbf{v}^{(l)}, T^{(l)}, V)$ are listed in the following table

Arc subregion	v_r	v_z	h or T	V
A^aB^a	0	$\frac{\partial v_z}{\partial r} = 0$	$\frac{\partial h}{\partial r} = 0$	$\frac{\partial V}{\partial r} = 0$
B^aC^a	0	0	$T = 3000K$ $(q_c = J_c V_c)$	$J_c = \frac{I}{\pi R_c^2}$
C^aD^a	0	0	$T = 3000K$	$\frac{\partial V}{\partial z} = 0$
D^aE^a	0	0	$T = 3000K$	$\frac{\partial V}{\partial r} = 0$
E^aF^a	0	$\rho\frac{\partial v_z}{\partial z} = 0$	$T = 1000K$	$\frac{\partial V}{\partial z} = 0$
F^aG^a	$\frac{\partial v_r}{\partial r} = 0$	$\frac{\partial v_z}{\partial z} = 0$	$T = 1000K$	$\frac{\partial V}{\partial r} = 0$
G^aH^a	$\frac{\partial v_r}{\partial r} = 0$	$\frac{\partial v_z}{\partial z} = 0$	$\frac{\partial h}{\partial r} = 0$	$\frac{\partial V}{\partial r} = 0$
H^aI^a	0	0	$T = 1000K$	$V = \text{const}$
I^aA^a	0	0	$T = 1000K$	$V = \text{const}$

Boundary conditions for Choo's et al model [9] in the weld pool subregion, shown in **Fig. 5**, are listed in the following table

Weld pool subregion	v_r	v_z	T	V
A^pB^p	0	$\frac{\partial v_z}{\partial r} = 0$	$\frac{\partial T}{\partial r} = 0$	$\frac{\partial V}{\partial r} = 0$
B^pC^p	0	0	$\frac{\partial T}{\partial r} = 0$	$\frac{\partial V}{\partial r} = 0$
C^pD^p	0	0	$T = 288K$	$\frac{\partial V}{\partial z} = 0$
D^pE^p	0	0	$T = 288K$	0
E^pF^p	0	0	$\frac{\partial T}{\partial z} = -q_a$	$J_a = -\sigma^{(e)}\frac{\partial V}{\partial z}$
F^pA^p	$\eta\frac{\partial v_r}{\partial z}\|_l = \frac{\partial\gamma}{\partial T}\frac{\partial T}{\partial r}$	0	$-k\frac{\partial T}{\partial z} = -q_a + q_{vap}$	$J_a = -\sigma^{(e)}\frac{\partial V}{\partial z}$

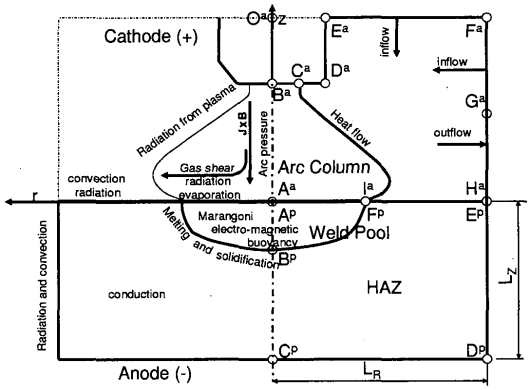

Fig. 8 Boundary conditions for the plasma discharge model proposed by Choo, Szekely and Westhoff [9]

3.5 Scheme for transferred arc in plasma arc welding (PAW) proposed by Aithal, Subramaniam, Pagan and Richardson [2]

The model of the transferred plasma arc consists of two regions: the internal flow within a torch, and the external jet impinging on the surface of a work-piece. Such model is applied to plasma arc welding (PAW) and is presented in [2], [3] and [4].

The discharge in plasma arc welding (PAW) is initiated between the inner electrode - cathode and the constricting nozzle - anode. It is initiated by applying a high frequency voltage superimposed on a dc bias between electrodes. The main arc - transferred arc, is subsequently struck between the workpiece (grounded) and the inner electrode by transferring the discharge. The inner cathode is biased negative with respect to the workpiece - anode, by approximately 30V.

The fundamental assumptions of PAW model [2] are listed in the table below

1	plasma flow is laminar, the maximum of Reynold's number for the transferred arc is less then 100
2	plasma consists of neutral Ar atoms, singly ionized atoms, and electrons
3	workpiece is considered a boundary of the fluid domain
4	modelling of the arc is not coupled with the weld pool
5	plasma is assumed to be quasi-neutral, i.e., $n^{(i)} \approx n^{(e)}$
6	sheath regions adjacent to electrodes are not considered
7	standard assumptions for MHD flow are assumed
8	plasma geometry is two-dimensional and axisymmetric
9	only the azimuthal component of the magnetic induction, B_θ, is significant
10	single temperature can represent the plasma
11	the above justifies the assumption of the local thermodynamic equilibrium (LTE)

The problem is formulated using the compressible Navier-Stokes equations that include the Lorentz force terms: $J_z B_\theta$ and $J_r B_\theta$, in momentum conservation equations and additional terms in the energy equation representing ohmic heating and work done by the Lorentz body forces. Equations controlling the internal and external plasma flow in PAW are shown in **Fig. 11**.

Boundary conditions for two sub-domains: internal and external, are shown in **Fig. 9** and **Fig. 10**.

The boundary conditions for the internal flow problem are listed in the following table

Region	ρ	v_r	v_z
ABCD	$\frac{\partial \rho}{\partial r} = 0$	0	0
DE	$m_a(n^{(e)} + n_a)$	$\frac{\partial^2 v_r}{\partial z^2} = 0$	$\frac{\partial^2 v_z}{\partial z^2} = 0$
EF	$\frac{\partial \rho}{\partial r} = 0$	0	$\frac{\partial v_z}{\partial r} = 0$
FGH	$\frac{\partial \rho}{\partial r} = 0$	0	0
HA	$m_a(n^{(e)} + n_a)$	0	$\frac{\partial^2 v_z}{\partial z^2} = 0$

Region	T	$n^{(e)}$	B_θ
ABCD	$\frac{\partial T}{\partial r}\|_{r=r_0} = a_1(T\|_{r=r_0} - T_{co})$, $a_1 = -0.0347[m]$, $T_{co} = 300K$	$\frac{\partial^2 n^{(e)}}{\partial r^2} = 0$	
DE	$\frac{\partial^2 T}{\partial z^2} = 0$	$\frac{\partial^2 n^{(e)}}{\partial z^2} = 0$	$\frac{\partial B_\theta}{\partial r} = 0$
EF	$\frac{\partial T}{\partial r} = 0$	$\frac{\partial n^{(e)}}{\partial r} = 0$	0
FGH	$\frac{\partial^2 T}{\partial r^2} = 0$	$\frac{\partial^2 n^{(e)}}{\partial r^2} = 0$	
HA	T_0	$\frac{\partial^2 n^{(e)}}{\partial z^2} = 0$	
GBCD			$B_\theta = \frac{\mu_0 I}{2\pi r}$
FG			$B_\theta = \frac{r\mu_0 I}{2\pi r_{ca}^2}$

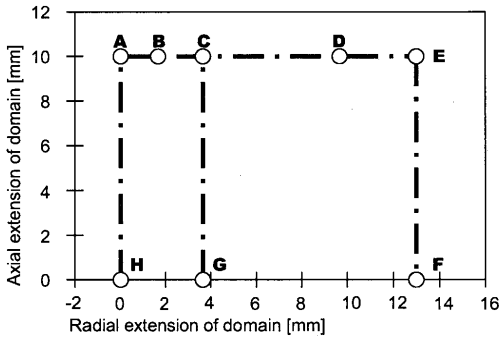

Fig. 9 The domain for the external plasma flow problem

Boundary conditions for the external flow problem are listed below

Region	ρ	v_r	v_z
AB	Sol.IFP	Sol.IFP	Sol.IFP
BD	$m_a(n^{(e)} + n_a)$	$-v_z \tan[\alpha(r)]$	qadr. distr. of v_z such that $\int_{r_1}^{r_2} v_z r dr = 0.1127[m^3/h]$
DE	$m_a(n^{(e)} + n_a)$	0	0
EF	$m_a(n^{(e)} + n_a)$	$\frac{\partial^2 v_r}{\partial r^2} = 0$	$\frac{\partial^2 v_z}{\partial r^2} = 0$
FH	$\frac{\partial \rho}{\partial z} = 0$	0	0
HA	$\frac{\partial \rho}{\partial r} = 0$	0	$\frac{\partial v_z}{\partial r} = 0$

Region	T	$n^{(e)}$	B_θ
AB	Sol.IFP	Sol.IFP	Sol.IFP
BD	500 K	Sol.IFP	
DE	500 K	$\frac{\partial^2 n^{(e)}}{\partial r^2} = 0$	
EF	$\frac{\partial T}{\partial r} = 0$	$\frac{\partial^2 n^{(e)}}{\partial r^2} = 0$	
FH	$\frac{\partial T}{\partial z} = -a_1(T\|_{z=L} - T_{pl})$ $a_1 = 75e^{\frac{-5r}{r_0}}[\frac{1}{m}]$ $r_0 = 12.7[mm]$ $T_{pl} = 500K$	$\frac{\partial n^{(e)}}{\partial z} = 0$	
HA	$\frac{\partial T}{\partial r} = 0$	$\frac{\partial n^{(e)}}{\partial r} = 0$	
BC			$\frac{\mu_0 I}{2\pi r}$
CG			$\frac{\mu_0 I}{2\pi r_{cath}}$
GH			$\frac{\partial B}{\partial z} = 0$
AH			0

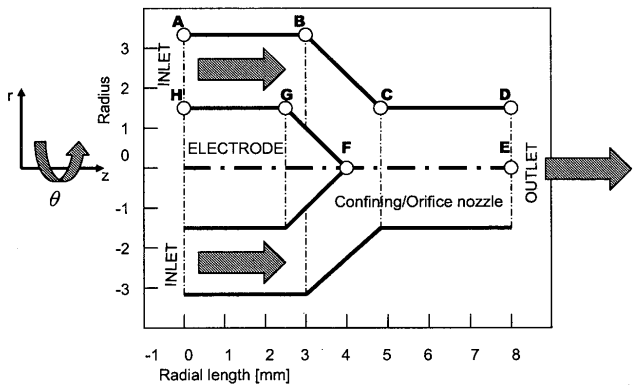

Fig. 10 The domain for the internal plasma flow problem

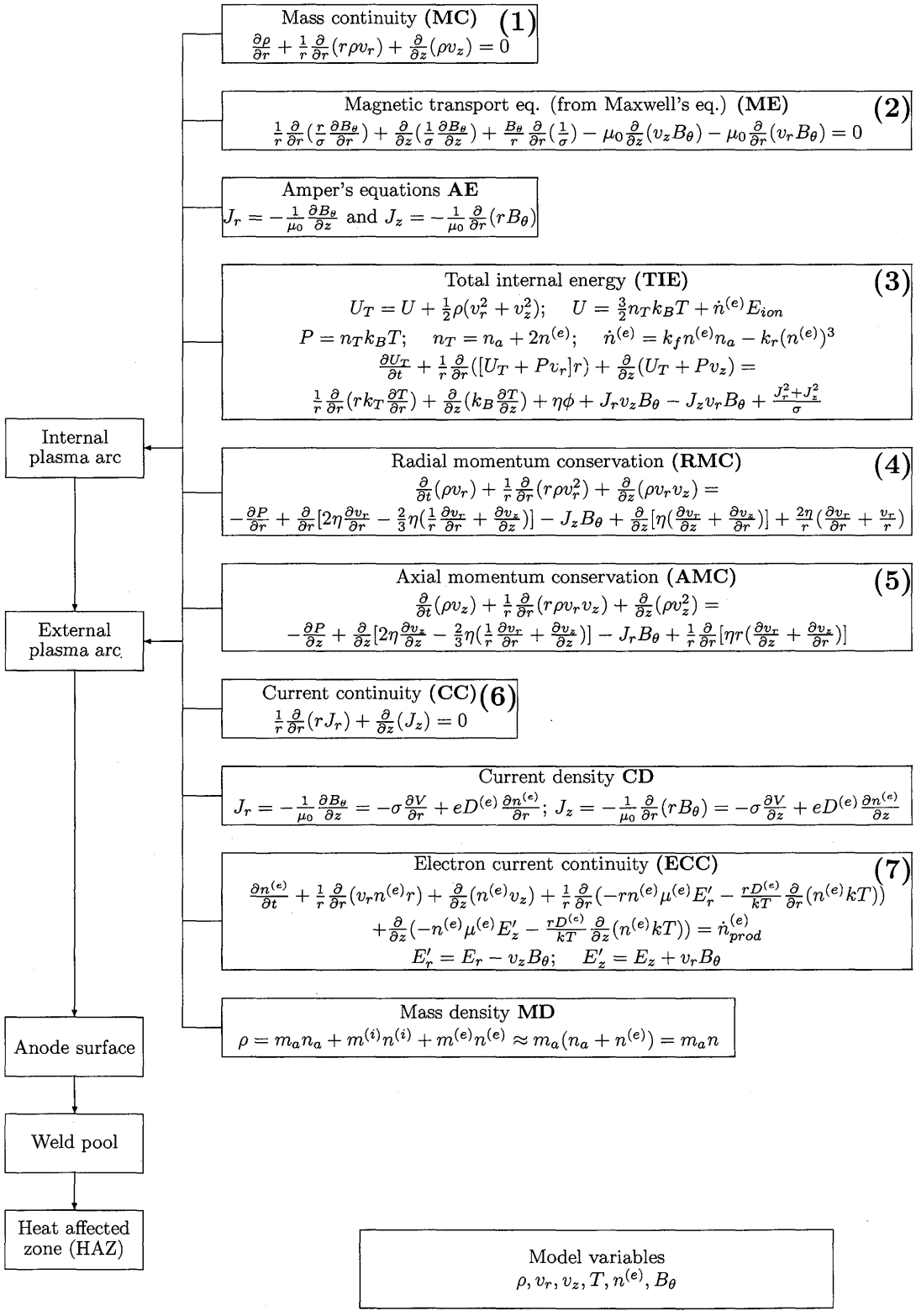

Fig. 11 The scheme for the model of plasma arc welding (PAW) proposed by Aithal, Subramaniam, Pagan and Richardson [2]

4 Thermal spraying

4.1 General information

Thermal spraying is the common name for a group of processes where finely ground powder of metallic or non-metallic materials or a reacting gas (methane) or a droplet of melted wire is accelerated to high velocities through either a combustion flame or dc or rf thermal plasma arc. Pieces injected or formed (eg. in the case of diamond coating) in a plasma jet, are in a molten, semi-molten or solid state and they are deposited on a prepared substrate. The substrate coating is developed by successive impingement and bonding of thin splats. Energy transfer in plasma spraying can be split into three successive stages:

- transfer of energy of an electrical potential field to a plasma gas manifested by ionization and plasma heating,
- heat and momentum transfer from the plasma to injected powder particles,
- transfer of thermal and kinetic energy from particles to a substrate.

The process can be characterized by the following unique features [52]

- various types of materials, ranging from metal through ceramics to polymers, and any combination of them, can be created,
- mixtures of components with a wide range of vaporization pressures can be deposited without significant changes in coating composition,
- homogeneous coatings with time invariant changes in composition can be produced,
- in contrast to the electron-beam technique, microstructure with fine, equiaxial grains and without columnar defects can be deposited,
- graded coatings with a smooth variation in a ceramic-metal mixture composition can be produced,
- high deposition rates can be achieved,
- the process can be conducted in air, reduced pressure, inert gas, and underwater.

Properties of coating, produced on a substrate, depend on five controllable groups of process variables [16]:

- the jet formation for a flame or a plasma that is related to the torch design, a combustible gas or shielding gas composition and mass flow rate, the dissipated power and many other process parameters.
- the powder chemical composition, particle size distribution, and its injection, powder morphology, injector internal diameter, shape, length, position, torch tilting and hose length, granule hidden trajectory between the powder feeder and the injector,
- composition of enveloping air or inert gas at pressure $\leq 10^5$ Pa,
- substrate material and its surface preparation: eg. cleanliness and roughness, oxidation, preheating, temperature, temperature control during and after spraying,
- relative motion of the torch and substrate that controls the coating thickness deposited per pass and, to some extent, the heat transfer to coating and substrate.

Main plasma spray parameters controlled at preset levels are shown in table:

Region	Parameter
Workpiece (substrate)	temperature residual stress particle quenching rate
Plasma	gas composition heat content plasma stream temperature velocity air dilution of plasma stream
Powder	particle size and shape distribution elemental distribution within particles dwell time in plasma stream
Powder injector	carrier gas
Plasma torch	relative movement workpiece stand-off

Types of thermal spraying processes are listed in the following table [26]:

Spraying process	Basic description
Combustion flame	uses compressed air or oxygen mixed with a fuel
High-velocity oxy-fuel (HVOF)	special torch design where a compressed flame undergoes free expansion upon exiting the torch nozzle, thereby experiencing high gas acceleration (over 4 Mach)
Two-wire electric-arc	two current-carrying, electrically conductive wires feed into a common arc point where melting occurs and the molten material is continuously atomized by compressed air, forming a molten spray with a high material throughput
Plasma spraying	A torch operates on direct current sustaining a stable, non-transferred electric arc between a water-cooled tungsten cathode and an annular, water-cooled cooper anode. An arc gas introduced at the back of the gun interior, swirls in a vortex and exitsout of the front of the nozzle. The arc glows between the cathode and the outer face of the anode and forms the exiting plasma flame.

Spraying process	Basic description
Radio-frequency (RF) induction	electrode-less thermal plasma is generated by inducing a current in the plasma gas.
Cold-spray technique	powder granules are accelerated in the supersonic gas stream produced by converging/diverging de Laval nozzle and the effect of hyper-velocity impact fusion occurs athermally when solid particles deform ballistically upon impact with a substrate or deposited layer.

4.2 Mathematical models of plasma spraying

Mathematical models of plasma spraying consist of two major sub-models:

- plasma jet,
- plasma-particle interaction.

One-, two- and three-dimensional models are restricted to specific techniques of spraying due to simplifying assumptions ignoring some important features of plasma-particle transport process. There is a large number of papers devoted to plasma spraying modelling and we will only study some of them which are representative of the various theories. We will discuss three plasma spraying theories proposed in [1], [6], [28], [31], [32], [42], [47].

4.2.1 One-dimensional theory [31]

The inflight particle parameters during plasma spraying can be predicted by a one-dimensional model [31]. This model accounts for the large temperature gradients and takes into consideration the Knudsen flow effect when the rate of flow does not depend on the viscosity of the gas for the model of gas flow in a container at a very low density. An injected granule of a powder is subjected to a varying temperature and experiences changes in thermo-physical gas properties. This model can be developed to be suitable for a high-velocity oxygen-fuel (HVOF) spraying process. It is assumed that a granule is spherical and the particle (granule) loading is low and does not affect the temperature and velocity of the plasma flame. The model consists of two processes of energy transfer:

- gas-particle heat transfer
  - heating of spherical particle

$$\rho_p c_p \frac{\partial T}{\partial t} = \frac{1}{r^2}\frac{\partial}{\partial r}(r^2 \kappa_p \frac{\partial T}{\partial r}) \qquad (15)$$

  - initial condition

$$T(r,t) = T_{p0} \quad \text{for} \quad t = 0, \quad r < \frac{d_p}{2}, \qquad (16)$$

  - boundary conditions for $t > 0$ at the particle surface

$$\frac{\partial T}{\partial r}|_{r=0} = 0$$

$$(\kappa_p \frac{\partial T}{\partial r})|_{r=\frac{d_p}{2}} = h(Nu)(T_g - T_{ps}) \qquad (17)$$

  - h(Nu) in Eq.17 is a function of the Nusselt number determined from Ranz-Marshall's correlation [48]

$$\mathrm{Nu} = \frac{h d_p}{\kappa_g^{itg}} = 2.0 + 0.514 Re^{\frac{1}{2}}, \qquad (18)$$

  - Reynolds number is

$$Re = d_p |v_p - v_g| \frac{\rho_g^{itg}}{\mu_g^{itg}} \qquad (19)$$

  - where κ_g^{itg} is defined by

$$\kappa_g^{itg} = \frac{1}{T_g - T_{ps}} \int_{T_{ps}}^{T_g} \kappa_g dT \qquad (20)$$

  - ρ_g^{itg} and μ_g^{itg} are defined by formulas like Eq. 20,
  - the Knudsen flow effect appears as the temperature jump at the granule surface $T_g > T_{pv}$ and then the temperature difference term $(T_g - T_{ps})$ in Eq.20 should be replaced by $\phi(T_g - T_{pv})$ where

$$\phi = 1 + 4\frac{2-\theta}{\theta}\frac{\Gamma_{ps}}{1+\Gamma_{ps}}\frac{\mathrm{Kn}}{\mathrm{Pr}_{ps}} \qquad (21)$$

- gas-particle momentum transfer
  - the corresponding equation can be written in the form of ODE for a granule velocity

$$\frac{dv_p}{dt} = \frac{3C_D(\mathrm{Re})\rho_g}{4 d_p \rho_p}(v_g - v_p)|v_g - v_p|, \qquad (22)$$

  - where C_D is corrected for the Knudsen effect by $\tilde{C}_D = C_D \phi^{0.45}$,
  - initial condition: $v_p = v_{p0}$ for $t = 0$,

4.2.2 Effects of plasma-injected granule interaction

The model, that can be seen as the extension of the concept [6] and the procedure described in [41], is proposed in [47] with the following assumptions:

Region	Assumption
plasma gas (argon under atmospheric pressure)	in local thermodynamic equilibrium (LTE), optically thin
flow	steady, laminar, axisymmetric, negligible viscous dissipation
electromagnetic field	one dimensional
injected particles	no particle-particle interactions, no internal heat transfer in the particle

The problem is described by energy and momentum balance laws, continuity and mass transfer equations, electromagnetic field equations, the particle trajectory equations, and initial and boundary conditions. Equations and laws as well as the information circulation between them is shown in **Fig. 12**, and the initial and boundary conditions are

- initial condition
  - all particles (granules) have zero initial radial velocity, i.e. $v_{pr}^{(0)} = 0$
- boundary conditions for the electromagnetic field set at $r = 0$ and $L_1 \leq z \leq L_2$

$$\chi = \frac{\pi}{2}$$
$$E_\theta = 0$$
$$B_z = B_{c\infty} \quad \{\frac{L_2 - z}{[R_c^2 + (L_2 - z)^2]^{1/2}} - \frac{L_1 - z}{[R_c^2 + (L_1 - z)^2]^{1/2}}\}$$

- total power input to the plasma $\mathcal{P}_0$ is specified as an integral boundary condition,

$$\mathcal{P}_0 = \alpha_c \mathcal{P}_t = 2\pi \int_{z=L_1}^{L_2} \int_{r=0}^{R_0} \mathcal{P} dr dz,$$
$$\text{where} \quad \alpha_c = (\frac{\mathcal{P}_0}{\mathcal{P}_t})^{1/2} \quad \text{should be specified,}$$

- boundary conditions for the plasma field
  - inlet conditions at $z = 0$

$$\begin{aligned} v_z &= 0, \\ v_r &= \frac{Q_1}{\pi r_1^1} \qquad r < r_1, \\ v_r &= 0 \qquad r_1 \leq r \leq r_2, \\ v_r &= \frac{Q_2}{\pi(r_3^2 - r_2^2)} \qquad r_2 \leq r \leq r_3, \\ v_r &= \frac{Q_3}{(R_0^2 - r_2^3)} \qquad r_3 \leq r \leq R_0, \\ T &= 350K, \\ y &= 0, \end{aligned}$$

  - centerline conditions at $(r = 0)$

$$\begin{aligned} v_z &= 0, \\ \frac{\partial v_r}{\partial r} &= 0, \\ \frac{\partial H}{\partial r} &= 0, \\ \frac{\partial y}{\partial r} &= 0, \end{aligned}$$

  - wall conditions at $r = R_0$

$$\begin{aligned} v_r &= v_z = 0, \\ \frac{\kappa}{c_p}\frac{\partial H}{\partial r} &= \frac{\kappa_c}{w}(T - T_{w0}), \\ \frac{\partial y}{\partial r} &= 0, \\ T_{w0} &= 350K, \end{aligned}$$

  - Exit conditions at $(z = L_T)$ for sufficiently large Peclet number i.e. $Re \cdot Pr$

$$\begin{aligned} \frac{\partial H}{\partial z} &= 0, \\ \frac{\partial v_z}{\partial z} &= 0, \\ \frac{\partial \rho v_r}{\partial z} &= 0, \\ \frac{\partial y}{\partial z} &= 0. \end{aligned}$$

The solution algorithm for this problem is:

- (step 1) compute electromagnetic fields: E_θ, H_z, and χ,
- (step 2) neglecting effects of injected particles, compute temperature T and velocity fields v_r, v_z for plasma,
- (step 3) evaluate plasma fields: T_p, v_{rp}, v_{zp},
- (step 4) calculate particle source terms: S_p^c, S_p^E, S_p^M,
- (step 5) evaluate new plasma fields: T^{i+1}, v_r^{i+1}, v_z^{i+1},
- repeat steps 3, 4 and 5 unless all field of plasma remain unchanged.

This model of plasma spraying can be used to investigate effects of particle size and loading, and carrier gas flow rate.

4.2.3 Wire-arc spraying model

In the wire-arc spraying process, the arc is struck between two metallic wires that melt as the wires are continuously fed through the torch head. A model describing the entire wire-arc spraying process is developed by Kelkar at. al. in [32] and consists of three parts: a gas dynamics model based on [8], an arc model following [33], and a plasma jet model proposed using the $(k - \varepsilon)$ turbulence concept [23]. The following simplifications are considered in this proposition:

- wire-arc spraying is the quasi-steady process,
- instabilities of the arc discharge and wire melting are not considered,
- the plasma is in LTE,
- the two-equation turbulence model $(k - \varepsilon)$ [23] is used in the plasma jet to predict the influence of small scale eddies on the mean flow,

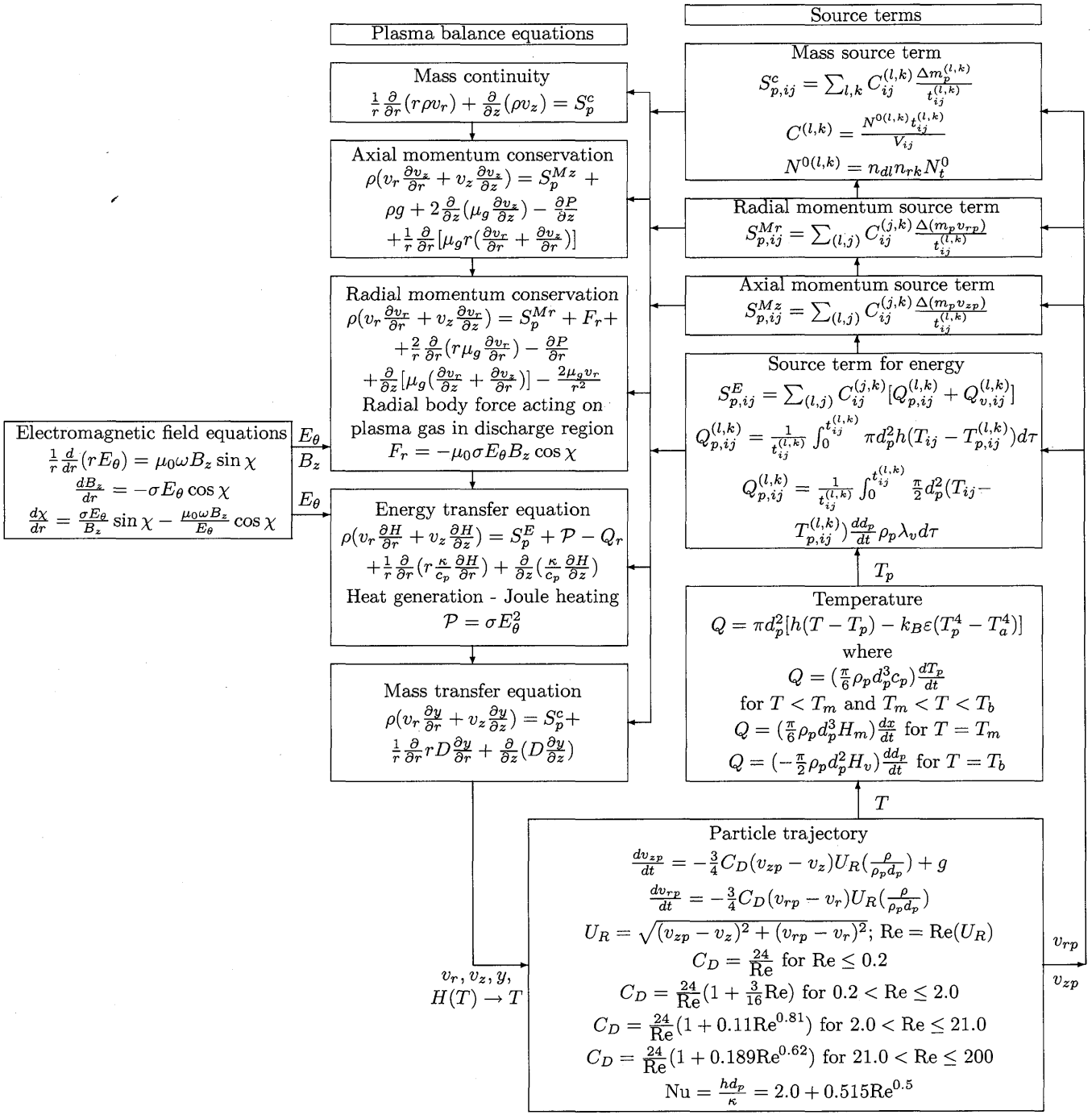

Fig. 12 The scheme for the model of plasma spraying proposed by Proulx at. al. [47]

- the effect of metal vapor, produced in the area of electrode wires, on flow variables of plasma is neglected,
- the effect of oxidation of molten droplets is also neglected,
- the deposition process of molten droplets on the substrate is not modelled.

Regions appropriate for the three sub-models are depicted in **Fig. 13**.

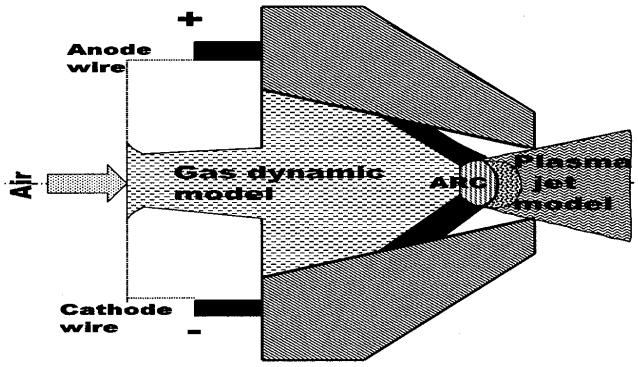

Fig. 13 Regions corresponding to sub-models for the wire-arc spraying process

The three sub-models are developed for various geometries:

Model	Dimension	Coordinate system
gas dynamics model	3-D	curvilinear coordinates $(x_i, i = 1, 2, 3)$
arc model	3-D	cylindrical (r, z, θ)
plasma jet model	3-D	Cartesian coordinates $x, y.z$

Unfortunately, the authors of [32] do not show how the corresponding model variables commute.
Variables of sub-models: density, velocity, temperature (enthalpy), and characteristics of electrical field, are calculated sequentially and the mathematical model of wire-arc spraying is shown in **Fig.14**
An electric arc interacts with a cross flow of air and due to this disturbance the arc becomes concave facing the upstream direction and the air stream loses symmetry and becomes three-dimensional. The arc model is developed with the following simplifications:

- plasma is in LTE,
- turbulence and instabilities occurring in the arc region are neglected,
- plasma is optically thin, i.e. the radiation from plasma is accounted for by using an optically thin radiation loss per unit volume,
- pressure variations are neglected,
- thermodynamic equilibrium and transport properties are assumed for plasma at pressure 100 kPa.

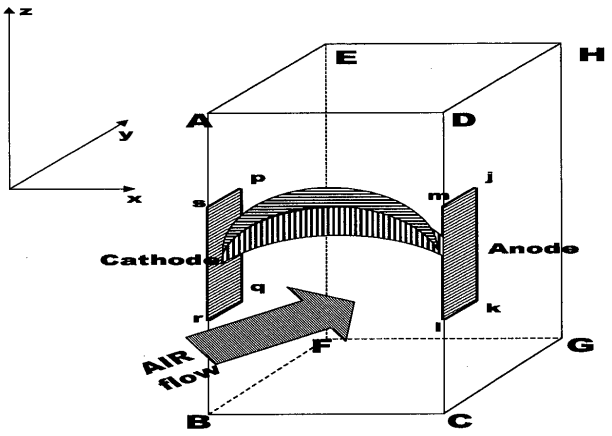

Fig. 14 Geometry of boundary conditions for the arc model

Boundary conditions for three sub-models are listed in the following table:

Sub-model	Boundary conditions
gas dynamics model	nozzle profile given in [32] inlet pressure 500 kPa, inlet temp. 300 K, exit velocity for the nozzle is 1.5 - 1.0 Ma
arc model	wire electrodes approximated by 3-3 mm areas [pqrs] and [jklm], order of spacing between electrodes is a few mm, temp. of [pqrs] cathode is 3000 K, current density distribution imposed on [pqrs] is constant in y-direction and in z-direction is defined by $j = j_{max} \exp(-b\|z - z_c\|)$, $b = 1.93mm^{-1}$, temperature of anode [jklm] is given by measurements in [27], anode is iso-potential surface, temperature of inflowing gas on face [ABCD] is 1000 K, temperature of inflowing gas is specified, normal velocity of gas at face [EFGH] ensures the global mass conservation, no current leakages are allowed outside of the numerical boundaries apart from electrodes, normal component of velocity is zero at the numerical boundaries

This mathematical model of spraying can be improved by including one of the semi-empirical sub-models for particle break-up and transport. These sub-models can be split into four parts: cathode primary breakup, anode primary break-up, droplet flow, and secondary breakup.

5 Notations used in schemes

Symbols used in the schemes for TIG thermal plasma, which follow the recommendations of the IUPAP-25 document [11] and NRL Plasma Formulary [29], are described in the following tables:

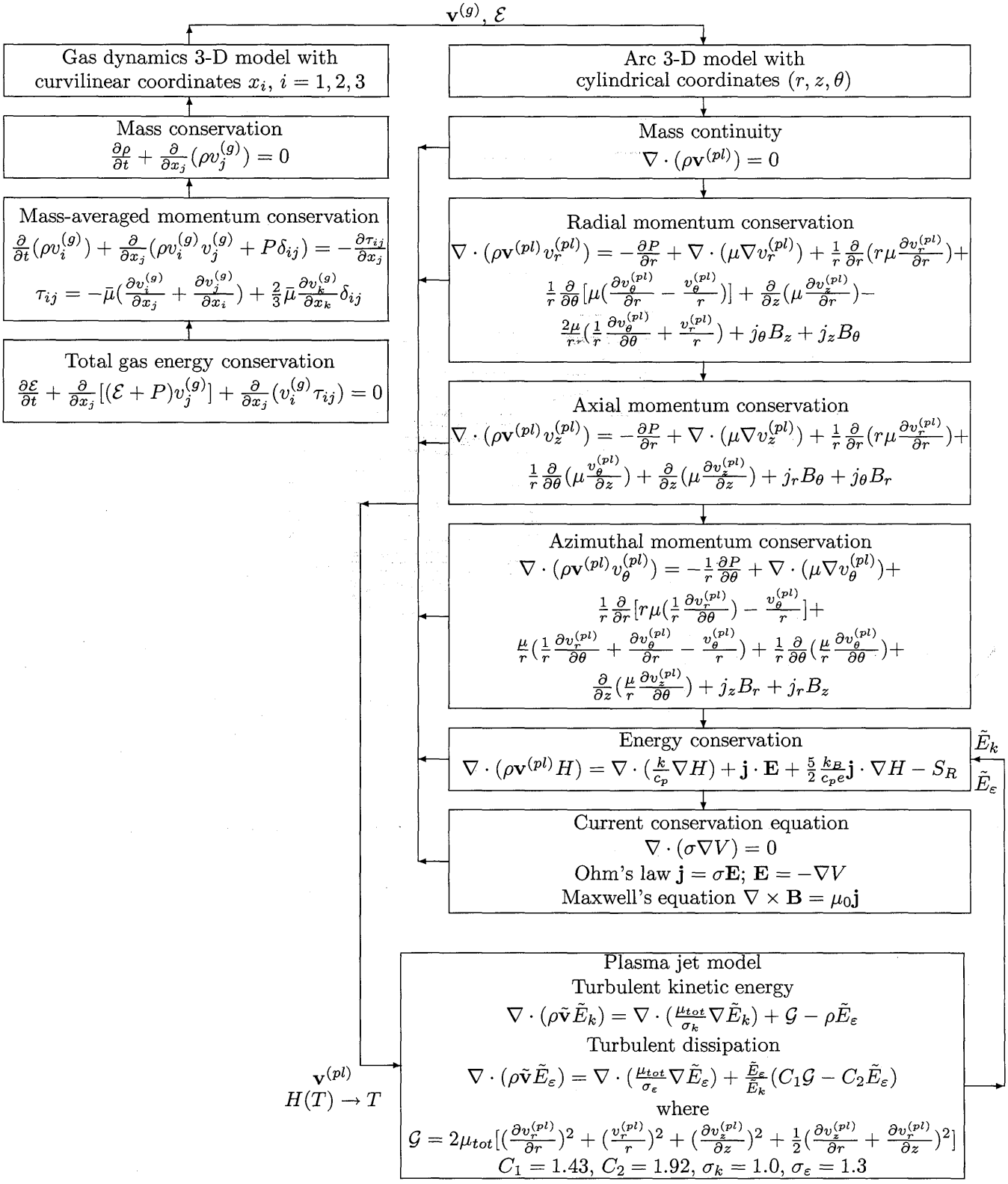

Fig. 14 The scheme for the model of wire-arc spraying proposed by Kelkar at. al. [32]

Symbol	Description
A	thermionic emission constant for a surface of cathode
A_R	Richardson's constant
B_θ	azimuthal magnetic field
B_z	axial magnetic field intensity
$B_{c\infty}$	magnetic field intensity for an infinite solenoid
c_p	specific heat at constant pressure
$C^{(i)}$	particle concentration of species $i = e, h, a$
$\overline{C_p}$, C_p	integrated mean heat capacity, heat capacity
$C_D(\mathrm{Re})$	drag coefficient, function of a granule Re
D	diffusion coefficient or thermal diffusivity (m^2/s)
D_{ia} $D^{(e)}$, D_{ee}	diffusion coefficient of ions in neutral atoms, thermal diffusion coefficient of electrons, self diffusion coefficient of electrons
D_{Mn-Ar}	binary diffusion coefficient of Mn in Ar gas
D_a	ambipolar coefficient
$D^{(e)}$	electron diffusion coefficient
d_p	sprayed granule diameter
e	elementary charge and also index for electrons
$\dot{E}_{eh}$	energy exchange
E_{ion} $E_{ion,r}$	ionization energy
E, $\mathbf{E}$	electric field
$E_r = \frac{\partial V}{\partial r}$ E_θ $E_z = -\frac{\partial V}{\partial z}$	radial, axial and circumferential components of the electric field
$\mathcal{E}$	total energy
E_k	turbulence energy in plasma jet model
E_ε	energy dissipated due to turbulence
f_l	fraction of fluid
g	acceleration due to gravity
g_r	statistical weight of excited state or multiplicity of energy state called also the degeneracy in Saha eq.: $r = 1$ for ions, $r = 0$ for neutrals
h	heat transfer coefficient
G	Saha function
H, $H^{(i)}$ $H^{(e)}$, H_w	total, ion, electron, and at wall enthalpy
(i, j)	location of a typical cell
J_{emi}, J_{rep} J_{tot} J_R, J_{ion} $J^{(i)}$, $J^{(e)}$ J_c, J_a	current density of emitted and repelled electrons total current density Richardson density, ions density accelerated towards cathode ion and electron current densities current density "to cathode" and "to anode"
$\mathbf{j}$	current density
k	entropy of vapor segregation
k_B	Boltzmann constant
k_f	rate constant for net production of electrons due to electron impact ionization defined in [40]
k_r	rate constant for net production of electrons due to three-body recombination defined in [40]
K, K_{max}	drag index and maximum drag index in the source term
Kn	Knudsen number
(l, k)	superscript: particles with initial diameter d_l and injected at radius r_k
l_{pp}	distance between plasma particles
L^i_{vap}	heat of vaporization of species i
L_r	boundary layer radius
L_1 L_2 L_T	lengths (dimensions) of torch
m_a, $m^{(e)}$ m_{ion}	mass of particle
$\Delta m_p^{(l,k)}$	amount of mass evaporated by a particle with (l, k) trajectory in cell (ij)
n, $n^{(e)}$ $n^{(i)}$	number densities: total, electron, ion
$\dot{n}^{(e)}_{prod}$	production of electrons due to chemical reactions, ionization and recombination
n_d	particle size distribution
n_r	represents the fraction of N_t^0 injected at each point over the central tube
$n^{(e)}_{sp}$ $n^{(e)}_{ed}$	density of electrons and ions at the sheath edge, density of plasma electrons at the sheath edge

Symbol	Description
n_a, n_r	number density of neutral atoms, in Saha equation: for $r = 1$ number density of ions, for $r = 0$ number density of neutral atoms
$(n^{(e)})^*$, n_a^*	number density of electrons and neutral atoms under conditions of LTE at T
N_t^0	total number of particles injected per unit time
$N^{0(l,k)}$	total number of particles pre unit time travelling along the trajectory (l, k) corresponding to a particle diameter d_p injected at the point r_k
Nu	Nusselt number
P	pressure
$\mathcal{P}$	$= \sigma E_\theta^2$ volumetric rate of heat generation due to Joule heating
Pr_w	Prandtl number at the boundary surface (wall)
Pr_w	Prandtl number $= \frac{C_p \eta}{k}$
Pr_w	Prandtl number at anode surface $= \frac{C_p \eta_{Ar}}{k}\|_{surf}$
Pr_{ps}	Prandtl number at a granule surface
q_a , q_c	energy flux density to anode and to cathode
$q_{a,elec}$ $q_{a,rad}$ $q_{a,conv}$	electronic, radiative, and convective contributions to energy flux density to anode
$q_{rad,i,j}$	radiative energy density flux received by surface element i from volume element j
q_{vap}	heat loss from cathode due to vaporization
Q	net heat exchange between a particle (granule) and its surrounding
Q_1	powder carrier gas flow rate
Q_2	plasma gas flow rate
Q_3	sheath gas flow rate
$Q^{(l,k)}_{p,ij}$	heat given to a particle
$Q^{(l,k)}_{v,ij}$	super-heat need to bring the particle vapors into thermal equilibrium with the plasma gas
$r_{i,j}$	direction vector from S_j to Ω_j
r, z	cylindrical coordinates
R	ideal gas constant
R_c	radius of cathode spot
S_r	differential surface in the radiation view factor relation
S_c	Schmidt number $= \frac{\nu}{D_{Mn-Ar}}$
S_R	radiation source, also heat lost due to radiation
$S_{R,i,j}$	plasma radiation emission coefficient
S_p^c	particle source term in continuity equation
S_p^E	particle source term in energy equation
S^{Mr}	particle source term in radial momentum equation
S^{Mz}	particle source term in axial momentum equation
$t_{ij}^{(l,k)}$	residence time of the (l, k) particles in the ij cell of volume V_{ij}
T,	temperature,
T_a	ambient temperature
T_c	cathode temperature
T_r	reference temperature for Bousinesq's approximation $(1523K)$
T_g	bulk combustion gas temperature
$T^{(e)}$ $T^{(e),a}$ $T^{(e)}_{ed}$, T_L, T_S	temperature of electron gas, temperature of electron gas at anode, temperature of the electron gas at the sheath edge, liquidus and solidus temperature
T_{p0}	initial particle temp. at the time of injection
T_{ps}	particle surface temperature
T_{pv}	temperature at the immediate granule vicinity
T_{wo}	external surface temperature of a tube (torch)
T_p T_m T_b	granule temperature melting point temperature boiling point temperature
u_{Bohm}	Bohm velocity
u	specific internal energy
U	radiation emission coefficient
U_T	total internal energy
U_R	relative speed between a granule and a plasma gas
v_r, v_z	axial and radial velocities
v_c	local speed of sound
v_g	plasma gas velocity
v_p	granule velocity
v_{p0}	granule injection velocity
v_r^e	radial velocity at the edge of anode boundary layer

Symbol	Description
$v_{pr}^{(0)}$	granule initial velocity
v_{gif}	flow at the region of input flow
$\bar{v}$	mean velocity of electron
$v_i^{(g)}$	gas velocity component
$v_r^{(pl)}$ $v_z^{(pl)}$ $v_\theta^{(pl)}$	components of plasma velocity
$V^{(i)}$	ionization potential of plasma
V, V_a V_c, V_{ed}	voltage, electric potential, anode fall voltage cathode fall voltage, voltage of electrons repelled
V_{ij}	cell (ij) volume
w	torch tube wall thickness
W	work function of the anode material
W_{eh}	energy exchange per volume unit due to elastic collisions of electrons with heavy particles
x	liquid fraction of a granule
y	particle vapor concentration
z_c	center of cathode
$\mathbf{A}$	vector potential for magnetic field
$\mathbf{B}$	magnetic field
$\mathbf{J}$	electric current density vector $\{J_r, J_z, J_\theta\}$
$\mathbf{q}^{(e)}$, $\mathbf{q}^{(h)}$	heat flux vector for electrons heat flux vector for ions
$\mathbf{u}^{(e)}$, $\mathbf{u}^{(i)}$	drift velocity for electron drift velocity for ions
$\mathbf{v}$	velocity vector $\{v_r, v_z, v_\theta\}$
α	$\alpha = 1 + 2\rho D^{(e)}/5n^{(e)}nm^{(e)}m_a D_{ee}$
α_c	correction factor to electric and magnetic field
α_{rec}	three-body recombination coefficient
γ	weld pool surface tension
$\mathbf{\Gamma}^{(e)}$ $\mathbf{\Gamma}^{(i)}$	 electron and ion fluxes
Γ_{ps}	specific heat ratio
δ_{ij}	Kronecker's delta (tensor)
ϵ	surface emissivity
$\varepsilon_L(\lambda_0)$	integrated volumetric emission coefficient
κ	total thermal conductivity
κ_c	thermal conductivity of quartz tube (torch)
κ_p	granule conductivity
κ_s	thermal conductivity for species
$\kappa^{(e)}$ $\kappa^{(h)}$	electron gas thermal conductivity heavy particle gas thermal conductivity
κ_g^{itg}	integral mean thermal conductivity
λ_0	wavelength [nm]
λ_v	latent heat of vaporization
η	viscosity
θ	thermal accommodation coefficient
μ_0	permeability of free space $= 4\pi \times 10^{-7}$ $[Hm^{-1}]$
μ_g	gas viscosity
μ_w	permeability of electrode material
μ_g^{itg}	integral mean values of gas viscosity
μ_{tot}	total viscosity containing both the laminar and turbulent (eddy) components
$\bar{\mu}$	mass-averaged viscosity coefficient
ν	kinematic viscosity
ν_c	collision frequency
ρ $\rho^{(e)}$ ρ_w	electron gas density ion mass density mass density in the edge of boundary layer
ρ_r	reference density for Bousinesq's approximation (7200 kg/m^2)
ρ_p	density of a granule material
ρ_g^{itg}	integral mean value of granule material density
σ $\sigma^{(e)}$	electrical conductivity of electron gas electrical conductivity
$\sigma(v)$	collision cross section
τ	shear stress tensor corresponding to strain rate tensor in [57] scheme
τ	relaxation time
Φ_c	Cathode work function, and coefficient of thermal diffusion for the electrons
Φ $\Phi^{(e)}$	effective work function of the electrode materials at room temperature
χ	phase angle $\chi = \phi_B - \phi_E$

Symbol	Description
ψ	angle between a direction of radiation and a surface unit vector
ω	oscillation frequency
ω_{sv}	specific volume
Ω_j ω_j	differential volume in the radiation view factor relation
w	subscript of values taken at the wall
swp	index for values taken on the surface of weld pool

References

[1] I. Ahmed and T.L. Bergman, Theree-dimansional simulation of thermal plasma spraying of partially molten ceramic agglomerates, *Journal of Thermal Spray Technology*, **9** 2000 215-224.

[2] S.M. Aithal, V.V. Subramaniam, J. Pagan and R.W. Richardson, Numerical model of a transfered plasma arc, *J. Appl. Phys.* **84** 1998 3506-3517.

[3] S.M. Aithal, V.V. Subramaniam and V. Babu, Comparison between numerical model and experiments for a direct current plasma flow, *Plasma Chemistry and Plasma Processing* **19** 1999 487-504.

[4] V. Babu, S.M. Aithal and V.V. Subramaniam, Numerical simulation of a hydrogen arcjet , *J. Propulsion Power* **12** 1996 1114-1122.

[5] M.I. Boulos, Heating of powders in the fire ball of an induction plasma, *IEEE Transactions in Plasma Science* **PS-6** 1978 93-106.

[6] M.I. Boulos, P. Fauchais and A. Vardelle, Fundamentals of plasma particle momentum and heat transfer, *Ed: Suryanarayanan, Plasma spraying: Theory and applications* (World Scientific Publishing, Singapore, 1993) 3-57.

[7] A. Capetti and E. Pfender, Probe measurements in argon plasma jets operated in ambient argon, *Plasma Chemistry and Plasma Processing* **9** 1989 329-341.

[8] G.V. Cendler and R.W. MacCormack, Computation of weakly ionized hypersonic flows in thermochemical nonequilibrium, *J. Thermophysics* **5** 1991 266-273.

[9] R.T.C. Choo, J. Szekely and R.C. Westhoff, Modelling of high-current arcs with emphasis on free surface phenomena in the weld-pool, *Welding Research Supplement* **September** 1990 346-361-s.

[10] R.T.C. Choo and J. Szekely, Vaporization kinetics and surface temperature in a mutually coupled spot gas tungsten arc weld and weld pool, *Welding Research Supplement* **March** 1992 77-93-s.

[11] E.R. Cohen and P. Giacomo, Symbols, units, nomenclature and fundamental constants in

physics, *Document IUPAP-25*, (International Union of Pure and Applied Physics, 1987)

[12] J.B. Cox and F.J. Weinberg, On the behaviour of enthalpy probes in fluctuating temperature environments, *J. Phys. D: Appl. Phys.* **4** 1971 877-881.

[13] L.E. Drain, *The laser Doppler technique* (Wiley, New York, 1980).

[14] W. Elenbaas, Die quecksilberhochdruckenladung, *Physica* **1** 1934 673-688.

[15] A.J.D. Farmer and G.N. Haddad, Rayleigh scattering measurements in a free-burning argon arc, *J. Phys. D: Appl. Phys.* **21** 1988 426-431.

[16] P. Fauchais, A. Vardelle and B. Dussoubs, Quo vadis thermal spraying, Eds. C.C. Berndt, K.A. Khor and E.F. Lugscheider, *Thermal Spray 2001: New surfaces for a new millenium, Published by ASM International, Materials Park, Ohio, USA, 2001*, 1-32.

[17] G. Gouesbet, A review on measurements of particle velocities and diameters by laser techniques, with emphasis on thermal plasmas *Plasma Chemistry and Plasma Processing* **5** 1985 91-117.

[18] G. Gregori, J. Schein, P. Schwendinger, U. Kortshagen, J. Haberlein, and E. Pfender, Thomson scattering measurements in atmospheric plasma jets, *Physical Review E* **59** 1999 2286-2291,

[19] J. Grey, P.F. Jacobs and M.P. Sherman Calorimetric probe for the measurement of extremely high temperatures, *Review for Scientific Instrumentations* **33** 1962 738-741.

[20] G.N. Haddad and A.J.D. Farmer, Temperature measurements in gas tungsten arcs, *Welding Research Suplement* **December** 1985 339s-342s.

[21] J. Haidar and J.J. Lowke, Predictions in metal droplet formation in arc welding, *J. Phys. D: Appl. Phys.* **29** 1996 2951-2960.

[22] J. Haidar, Local thermodynamic equilibrium in the cathode region of a free burning arc in argon, *J. Phys. D: Appl. Phys.* **28** 1995 2494-2504.

[23] F.H. Harlow and P.I. Nakayama, Turbulence transport equations, The Physics of Fluids, **10** 1967 2323-2332.

[24] R.B. Heimann, *Plasma-spray coating* (VCH, Weinheim, 1996)

[25] G. Heller, Dynamical similarity laws of the mercury high pressure discharge, *Physics* **6** 1935 389-394.

[26] H. Herman, S. Sampath and R. McCune, Thermal spray: current status and future trends, *MRS Bulletin* **July** 2000 17-25.

[27] K.C. Hsu, K. Etemadi and E. Pfender, Study of the free-burning high-intensity argon arc, *J. Appl. Phys.* **54** 1983 1293-1301.

[28] P.C. Huang, J. Haberlain and E. Pfender, A two-fluid model of turbulence for thermal plasma jet, *Plasma Chemistry and Plasma Processing* **15** 1995 25-46.

[29] J.D. Huba, NRL plasma formulary, *The Office of Naval Research* 1994.

[30] I. H. Hutchinson, *Principles of plasma diagnostics*(I.H. Huthinson, 2002).

[31] S.V. Joshi and R. Sivakumar, An analytical approach to plasma spraying, *Ed: Suryanarayanan, Plasma spraying: Theory and applications* (World Scientific Publishing, Singapore, 1993) 121-137.

[32] M. Kelkar and J. Heberlain, Wire-arc spray modelling, *Plasma Chemistry and Plasma Processing* **22** 2002 1-25.

[33] M. Kelkar and J. Heberlein, Physics of an arc in cross flow, *J. Phys. D: Appl. Phys.* **33** 2000 2172-2182.

[34] P. Kovitya and J.J. Lowke, Two-dimensional analysis of free burning arcs in argon, *J. Phys. D.: Appl. Phys.* 1985 53-70.

[35] S. Kuroda, T. Fukushima, S. Kitahara, H. Fujimori, Y. Tomita and T. Horiuchi, Monitoring of thermally sprayed particles using thermal radiation, Ed. I.A. Bucklow, *Thermal spraying : current status and future trends : Proceedings of the 12th International Thermal Spray Confernce, 4-9 June, 1989, London* P27-1 - P27-9.

[36] C. Lao, J. Cotrino, A. Palmero, A. Gamero, and A.R. Gonzalez-Elipe, Electron temperature measurement in a surface-wave-produced argon plasma at intermediate pressures, *Eur. Phys. J. D* **14** 2001 361-366.

[37] J. Lesinski and M.I. Boulos, Laser Doppler under plasma conditions. Part 1: Measurements in a d.c. plasma jet, *Plasma Chemistry and Plasma Processing* **8** 1988 113-132,

[38] J. Lesinski and M.I. Boulos, Laser Doppler under plasma conditions. Part 2: Measurements in an inductively coupled r.f. plasma, *Plasma Chemistry and Plasma Processing* **8** 1988 133-144.

[39] H. Maecker, Uber die charakteristiken zylindrischer bogen, *Zeitschrift fur Physik* **157** 159 1-29.

[40] P. Mensbach and J. Keck, Monte Carlo trajectory calculation at atomic excitation and ionization by thermal electrons, *Physical Review* **181** 1969 275-289.

[41] J. Mostaghimi, P. Proulx and M.I. Boulos, An analysis of the computer modelling the flow and temperature fields in an inductively coupled plasma, *Numerical Heat Transfer* **8** 1985 187-201.

[42] W.L. Oberkampf and M. Talpallikar, Analysis of high-velocity oxygen-fuel (HVOF) thermal spray torch, Part 1: Numerical formulation, *Journal of Thermal Spray Technology* **5** 1996 53-61.

[43] S.V. Patankar and D.B. Spalding, *Heat and Mass Transfer in Boundary Layers* (Intertext Books, London, 1970).

[44] S.V. Patankar and D.B. Spalding, A calculation procedure for heat, mass, and momentum transfer in three-dimensional parabolic flow, *Int. J. Heat Mass Transfer* **15** 1972 1787-1806.

[45] S.V. Patankar, A calculation prcedure for two-dimensional elliptic situations, *Numerical Heat Transfer* **4** 1981 409-425.

[46] D. Poirier and C. Boucher, Validation of plasma velocity measurements with Mach probes using laser induced fluorescence *Ed. P. Pavlo, Controled fusion and plasma physics, 25th Europ. Conf., Prague, ECA* **22 C** 1998 1602-1605.

[47] P. Proulx, J. Mostaghimi and M.I. Boulos, Plasma-particle interaction effects in induction plasma modelling under dense loading conditions, *Int. J. Heat and Mass Transfer*, **28** 1985 1327-1336.

[48] W.E. Ranz and W.R. Marshall, Evaporation from drops, Part 1, *Chem. Enging. Prog.* **48** 1952 141-146.

[49] J. Ronda, H. Murakawa, K. Nogi and M.Ushio, Enhanced method of heat sources in welding and plasma spraying (1st Report) - Overview of simple thermal plasma models, *Trans. JWRI* **31** 2002 1-11.

[50] A. Rutscher, *Plasmatechnik, Grundlagen und Anwendungen, Eine Einfuhrug*, (Carl Hanser-Verlag, Munchen, Wien, 1982).

[51] L. Sansonnens, J. Haidar and J.J. Lowke, Prediction of properties of free burning arcs including effects of ambipolar diffusion, *J. Phys. D: Appl. Phys.* **33** 2000 148-157.

[52] R.W. Smith and R. Novak, Advances and applications in U.S. thermal spray techology. I. Technology and materials, *Powder Metallurgy International* **23** 1991 147-155.

[53] M. Thorpe, Plasma energy: the ultimate in heat transfer, *Chemical Engineering Progress* **85** 1989 48-53.

[54] J.P. Van Doormaal and G.D. Raithby, Enhancements of the simple method for predicting incompressible fluid flow, *Numerical Heat Transfer* **7** 1984 147-163.

[55] M. Vardelle, A. Vardelle, P. Fauchais and M.I. Boulos, Plasma-particle momentum and heat transfer: Modelling and Measurements, *AIChE Journal* **29** 1983 236-243.

[56] M. Vardelle, A. Vardelle, P. Fauchais and M.I. Boulos, Particle dynamics and heat transfer under plasma conditions, *AIChE Journal* **34** 1988 567-573.

[57] J. Wendelstorf, I. Decker, H. Wohlfahrt and G. Simon, TIG and plasma arc modelling: A survey, in: H. Cerjak (Ed.), Mathematical Modelling of Weld Phenomena, The Institute of Materials, London, 1997, 848-897.

[58] J. Wendelstorf, Ab initio modelling of thermal plasma gas dischargers (electric arcs), Ph.D. Thesis, TU Braunschweig, 2000.